Rigorous Analysis of the Propagation Characteristics of General Lossless and Lossy Multiconductor Transmission Lines in Multilayered Media

Frank Olyslager, *Student Member, IEEE,* Daniël De Zutter, and Krist Blomme, *Student Member, IEEE*

***Abstract*— The frequency dependent propagation characteristics of lossless and lossy open coupled polygonal conductor transmission lines in a multilayered medium are determined based on a rigorous full-wave analysis. A boundary integral equation technique is used in conjunction with the method of moments. Losses in conductors and layers are included in an exact way without making use of a perturbation approach. Dispersion curves for the complex propagation constants and impedances are presented for a number of relevant examples and, where possible, compared with published data.**

I. Introduction

THE STRUCTURES analyzed in this paper consist of coupled polygonal waveguides in a multilayered medium. Though the theory is valid from pure dielectric to perfect conducting waveguides we will restrict ourselves to polygonal conductors. These conductors can be perfectly conducting or have a finite conductivity. As no simplifying assumptions have been introduced, our approach allows a rigorous study of skin effect phenomena.

Polygonal transmission lines have already been studied by a number of authors, however mostly restricted to the quasi-TEM limit. In [1] a quasi-TEM analysis is presented of coupled polygonal conductors in a layered medium. The authors use the Green's function of free space and the layered medium is taken into account by polarization charges at the layer interfaces. In [2] the same authors use a perturbation theory to include losses in layers and conductors. In [3] the same kind of structures were analysed in the quasi-TEM limit, however by means of the Green's function of the layered medium. Recently in [4] a complex image technique was proposed to handle the layered medium.

In [5] the rigorous full-wave analysis of open polygonal conductors is limited to the case of perfectly conducting conductors. The analysis is based on a mixed potential integral equation technique in conjunction with the Green's dyadic of the layered medium. The authors study the behavior of the propagation constants of the first and higher order modes in the bound and leaky regime. The propagation constants and impedances of perfectly conducting wire transmission lines in multilayered media were determined in [6]. Some authors have investigated the influence of finite thickness or losses of microstrip structures with perturbation techniques, for example in [7], [8].

Manuscript received January 7, 1992; revised May 1, 1992.

The authors are with the Laboratory of Electromagnetism and Acoustics, University of Ghent, Sint-Pietersnieuwstrant 41, 9000 Ghent, Belgium.

IEEE Log Number 9204027.

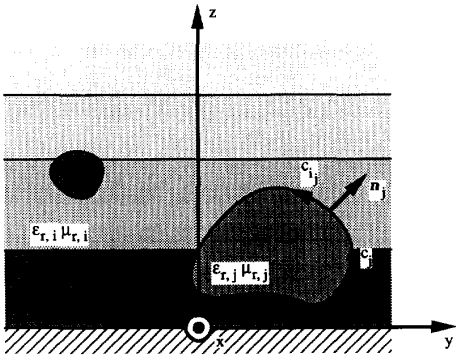

Fig. 1. Geometry of a general multiconductor transmission line.

To the authors knowledge this paper is the first rigorous analysis for both the propagation constants and impedance matrix of coupled polygonal transmission lines including losses and without any perturbation approach.

The general outline of the theory is developed for conductors with arbitrary cross-section. In the detailed calculations however, it becomes necessary to assume polygonal cross-sections. This assumption leads to considerable simplifications as a number of integrations can be carried out analytically.

The eigenmodes propagated along the structures under study are determined with a boundary integral equation technique. This integral equation is an extension of the equation used in [6]. The sources of the eigenmodes are the tangential electric and magnetic field components at the conductor boundaries. The integral equation is solved with the method of Galerkin. The eigenvalues of this integral equation are the propagation constants and the eigenvectors yield the modal fields. These modal fields are used to calculate the propagated power. From the propagated power we determine the impedance matrix.

II. Geometry of the Problem

Fig. 1 shows the geometry of the analyzed structures. There are L layers and we will use the subscript 'i' $(i = 1, \cdots, L)$ to refer to the ith layer. Each layer consists of homogeneous and isotropic material characterised by an arbitrary relative complex permittivity $\epsilon_{r,i}$ and complex permeability $\mu_{r,i}$.

A total number of C conductors are embedded in the layered medium and the subscript 'j' ($j = 1, \cdots, C$) refers to the jth conductor. Because a conductor can be located in more than one layer we use the notation C_i to indicate the total number of conductor parts in layer i while the subscript 'i_j' ($j = 1, \cdots, C_i$) refers to the jth conductor part in layer i.

Each conductor j consists of homogeneous and isotropic material characterized by an arbitrary relative permittivity $\epsilon_{r,j}$ and permeability $\mu_{r,j}$. The permittivity is a complex number and contains the conductivity σ of the conductor. In many cases one will deal with good conductors so that the real part of ϵ_r can be neglected and that $\epsilon_r = \sigma/j\omega\epsilon_0$. The case of perfectly conducting conductors is found by making ϵ_r infinite. The boundary of conductor j is denoted by c_j. Note that c_{i_j} is the boundary of conductor part j in layer i. $\boldsymbol{n}_j$ is the external normal to c_j and $\boldsymbol{r}_j(y, z)$ is the position vector in the (y, z)-plane of a point on c_j.

III. Construction of the Integral Equation

A. Introduction

The common time and longitudinal dependence $e^{j(\omega t - \beta x)}$ in all field components, with ω the pulsation and β the propagation constant, is omitted. We use the longitudinal field components $E_x(\boldsymbol{r})$ and $H_x(\boldsymbol{r})$, with $\boldsymbol{r} = y\boldsymbol{u}_y + z\boldsymbol{u}_z$, as basis from which the other field components can be generated. The sources which build up these longitudinal field components are the tangential fields $\boldsymbol{n}_j \times \boldsymbol{E}(\boldsymbol{r}_j)$ and $\boldsymbol{n}_j \times \boldsymbol{H}(\boldsymbol{r}_j)$ at the boundaries of the conductors. These tangential fields consist of longitudinal contributions $E_{x,j}(\boldsymbol{r}_j)$ and $H_{x,j}(\boldsymbol{r}_j)$ along the conductors and transversal contributions $E_{t,j}(\boldsymbol{r}_j)$ and $H_{t,j}(\boldsymbol{r}_j)$ in the cross-section of the structure. The four functions $E_{x,j}(\boldsymbol{r}_j), H_{x,j}(\boldsymbol{r}_j), E_{t,j}(\boldsymbol{r}_j)$ and $H_{t,j}(\boldsymbol{r}_j)$ along all the conductor boundaries are the unknowns of the eigenmode problem and will be referred to as the sources in the sequel.

We will make a distinction between the so-called internal regions inside the conductors and the so-called external regions outside the conductors. The fields in both the external and internal regions are expressed as a function of the sources at the conductor boundaries. The fields in the external regions are the sum of incoming fields and scattered fields. The incoming fields are defined to be the fields generated by the sources if the layer, in which these sources are located, fills up whole space. These incoming fields however will reflect at the layer interfaces and penetrate into the other layers. In this way the scattered fields are generated. The incoming fields exist only in the layer of the sources while the scattered fields exist in all layers. The same partitioning of the fields was used in [6]. The internal and external regions are connected by imposing appropriate boundary conditions between the field expressions in both regions. This results in the final integral equation.

B. Internal Regions

Consider the internal region of conductor j shown in Fig. 2(a). From elementary electromagnetics it is known that the longitudinal fields in a homogeneous space are solution to the Helmholtz equation. From this fact, using Green's identity, it can be shown that the total longitudinal fields inside the conductor can be expressed as a contour integral along the boundary c_j:

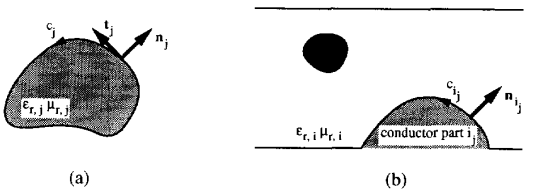

(a) (b)

Fig. 2. Internal region of conductor j (Fig. 2(a)) and external region in layer i around conductor part i_j (Fig. 2(b)).

$$
\begin{aligned}
E_{x,j}(\boldsymbol{r}) &= E^{\text{in}}_{x,j}(\boldsymbol{r}) \\
&= \oint_{c_j} \left[E_{x,j}(\boldsymbol{r}'_j) \frac{\partial G_j(\boldsymbol{r}|\boldsymbol{r}'_j)}{\partial n'_j} - G_j(\boldsymbol{r}|\boldsymbol{r}'_j) \frac{\partial E_{x,j}(\boldsymbol{r}'_j)}{\partial n'_j} \right] dc' \\
H_{x,j}(\boldsymbol{r}) &= H^{\text{in}}_{x,j}(\boldsymbol{r}) \\
&= \oint_{c_j} \left[H_{x,j}(\boldsymbol{r}'_j) \frac{\partial G_j(\boldsymbol{r}|\boldsymbol{r}'_j)}{\partial n'_j} - G_j(\boldsymbol{r}|\boldsymbol{r}'_j) \frac{\partial H_{x,j}(\boldsymbol{r}'_j)}{\partial n'_j} \right] dc'.
\end{aligned}
\tag{1}
$$

Because these total fields are analogous to the external incoming fields (2) discussed in the next subsection we explicitely introduced the superscript 'in' in (1). This will simplify the subsequent discussion. $G_j(\boldsymbol{r}|\boldsymbol{r}')$ is the two-dimensional Green's function of homogeneous space filled with the material of the conductor. From the knowledge of $E_{x,j}$, $H_{x,j}$ and their normal derivatives at the boundary c_j we can calculate $E_{x,j}$ and $H_{x,j}$ everywhere inside the conductor.

C. External Regions

Now consider layer i in which some conductor parts are located (Fig. 2(b)). First we concentrate on conductor part i_j. The incoming fields generated in layer i by this conductor part are given by

$$
\begin{aligned}
&E^{\text{in}}_{x,i_j}(\boldsymbol{r}) = \\
&- \oint_{c_{i_j}} \left[E_{x,i_j}(\boldsymbol{r}'_{i_j}) \frac{\partial G_i(\boldsymbol{r}|\boldsymbol{r}'_{i_j})}{\partial n'_{i_j}} - G_i(\boldsymbol{r}|\boldsymbol{r}'_{i_j}) \frac{\partial E_{x,i_j}(\boldsymbol{r}'_{i_j})}{\partial n'_{i_j}} \right] dc' \\
&H^{\text{in}}_{x,i_j}(\boldsymbol{r}) = \\
&- \oint_{c_{i_j}} \left[H_{x,i_j}(\boldsymbol{r}'_{i_j}) \frac{\partial G_i(\boldsymbol{r}|\boldsymbol{r}'_{i_j})}{\partial n'_{i_j}} - G_i(\boldsymbol{r}|\boldsymbol{r}'_{i_j}) \frac{\partial H_{x,i_j}(\boldsymbol{r}'_{i_j})}{\partial n'_{i_j}} \right] dc'
\end{aligned}
\tag{2}
$$

$G_i(\boldsymbol{r}|\boldsymbol{r}')$ now represents the Green's function corresponding to layer i. Remark that the signs in front of the integrals in (2) and (1) are different because the normal vector $\boldsymbol{n}$ is now pointing inward relative to the external region. The incoming fields will generate scattered fields in all layers of the structure. Now we can write down the total fields in each layer i:

$$
\begin{aligned}
E_{x,i}(\boldsymbol{r}) &= \sum_{j=1}^{C_i} E^{\text{in}}_{x,i_j}(\boldsymbol{r}) + \sum_{j=1}^{C} E^{sc}_{x,j}(\boldsymbol{r}) \\
H_{x,i}(\boldsymbol{r}) &= \sum_{j=1}^{C_i} H^{\text{in}}_{x,i_j}(\boldsymbol{r}) + \sum_{j=1}^{C} H^{sc}_{x,j}(\boldsymbol{r}),
\end{aligned}
\tag{3}
$$

where $E^{sc}_{x,j}(\boldsymbol{r})$ and $H^{sc}_{x,j}(\boldsymbol{r})$ are the scattered fields generated in the layered structure by all the conductor parts of conductor j. If there are no conductor parts in layer i, the total fields in this layer will only consist of scattered fields due to the conductors in the other layers.

D. Boundary Conditions and Unknown Sources

In the previous two sections it was demonstrated that it is sufficient to know the longitudinal field components and their normal derivatives at the conductor boundaries to know the electromagnetic fields everywhere. This suggests the use of $E_x(\boldsymbol{r}_j), H_x(\boldsymbol{r}_j), \partial E_x(\boldsymbol{r}_j)/\partial n$ and $\partial H_x(\boldsymbol{r}_j)/\partial n$ as basic unknowns in the eigenmode problem. However $\partial E_x(\boldsymbol{r}_j)/\partial n$ and $\partial H_x(\boldsymbol{r}_j)/\partial n$ are not suitable because they are not continuous and take different values at the inside and outside of the conductor boundaries.

To solve this problem we closely examine the continuity relations at the conductor boundaries. A first set of boundary conditions are the continuity of the longitudinal field components E_x and H_x. Secondly we have the continuity of the tangential field components E_t and H_t in the transverse (y,z)-plane.

In the local tangent coordinate system to curve c of Fig. 2(a) we can express E_t and H_t as a function of derivatives of E_x and H_x:

$$\begin{aligned} E_t &= -\frac{j\beta}{\gamma^2}\frac{\partial E_x}{\partial t} + \frac{j\omega\mu}{\gamma^2}\frac{\partial H_x}{\partial n} \\ H_t &= -\frac{j\beta}{\gamma^2}\frac{\partial H_x}{\partial t} - \frac{j\omega\epsilon}{\gamma^2}\frac{\partial E_x}{\partial n} \end{aligned} \tag{4}$$

with $\gamma^2 = \omega^2\epsilon\mu - \beta^2$.

Equation (4), which can be derived from Maxwell's equations, gives us expressions for the normal derivatives as a function of continuous quantities. Note in this respect that the continuity of E_x and H_x at the boundaries implies the continuity of their tangential derivatives. Consequently we will use $E_t, H_t, \partial E_x/\partial t$ and $\partial H_x/\partial t$ as basic unknowns instead of $\partial E_x/\partial n$ and $\partial H_x/\partial n$. If the functions E_x and H_x are known at the boundaries then $\partial E_x/\partial t$ and $\partial H_x/\partial t$ are also known by derivation along the boundary. Hence no new unknowns are introduced by these derivatives and the final set of unknown functions is E_x, H_x, E_t and H_t at the boundaries.

Replacing the normal derivatives of the fields in (1), using (4), results in

$$\begin{aligned} E^{\text{in}}_{x,j}(\boldsymbol{r}) &= \oint_{c_j}\left[E_{x,j}\frac{\partial G_j}{\partial n'_j} - G_j\left(\frac{j\gamma_j^2}{\omega\epsilon_j}H_{t,j} - \frac{\beta}{\omega\epsilon_j}\frac{\partial H_{x,j}}{\partial t'_j}\right)\right]dc' \\ H^{\text{in}}_{x,j}(\boldsymbol{r}) &= \oint_{c_j}\left[H_{x,j}\frac{\partial G_j}{\partial n'_j} - G_j\left(-\frac{j\gamma_j^2}{\omega\mu_j}E_{t,j} + \frac{\beta}{\omega\mu_j}\frac{\partial E_{x,j}}{\partial t'_j}\right)\right]dc' \end{aligned} \tag{5}$$

and an analogous replacement can be performed in (2).

E. Final Set of Integral Equations

The integral equations are constructed by connecting the internal and external regions. This means that we impose the continuity relations between the total fields at the outside and the total fields at the inside of the conductor boundaries. As explained in the previous subsection, it is sufficient to impose the continuity of the longitudinal components E_x and H_x and the tangential transversal components E_t and H_t:

$$\begin{aligned} &\lim_{\boldsymbol{r}\vec{>}\boldsymbol{r}_{i_o}}\left[\sum_{j=1}^{C_i}E^{\text{in}}_{x,i_j}(\boldsymbol{r}) + \sum_{j=1}^{C}E^{sc}_{x,j}(\boldsymbol{r})\right] \\ &= \lim_{\boldsymbol{r}\vec{<}\boldsymbol{r}_{i_o}} E^{\text{in}}_{x,o}(\boldsymbol{r}) \\ &\lim_{\boldsymbol{r}\vec{>}\boldsymbol{r}_{i_o}}\left[\sum_{j=1}^{C_i}H^{\text{in}}_{x,i_j}(\boldsymbol{r}) + \sum_{j=1}^{C}H^{sc}_{x,j}(\boldsymbol{r})\right] \\ &= \lim_{\boldsymbol{r}\vec{<}\boldsymbol{r}_{i_o}} H^{\text{in}}_{x,o}(\boldsymbol{r}) \\ &\lim_{\boldsymbol{r}\vec{>}\boldsymbol{r}_{i_o}}\left[\sum_{j=1}^{C_i}E^{\text{in}}_{t,i_j}(\boldsymbol{r}) + \sum_{j=1}^{C}E^{sc}_{t,j}(\boldsymbol{r})\right] \\ &= \lim_{\boldsymbol{r}\vec{<}\boldsymbol{r}_{i_o}} E^{\text{in}}_{t,o}(\boldsymbol{r}) \\ &\lim_{\boldsymbol{r}\vec{>}\boldsymbol{r}_{i_o}}\left[\sum_{j=1}^{C_i}H^{\text{in}}_{t,i_j}(\boldsymbol{r}) + \sum_{j=1}^{C}H^{sc}_{t,j}(\boldsymbol{r})\right] \\ &= \lim_{\boldsymbol{r}\vec{<}\boldsymbol{r}_{i_o}} H^{\text{in}}_{t,o}(\boldsymbol{r}) \qquad i_o = 1,\cdots,C_i \qquad i = 1,\cdots,L, \end{aligned} \tag{6}$$

where $\boldsymbol{r}_{i_o}$ is a position vector located on the oth conductor part in layer i. The subscript 'o' in the incoming fields at the right hand side refers to the conductor to which conductor part 'i_o' belongs. The limiting operation at the left hand side is performed from the external region to the conductor boundary as indicated by the notation '$\boldsymbol{r}\vec{>}\boldsymbol{r}_{i_o}$' and the operation at the right hand side is performed from the internal region is indicated by the notation '$\boldsymbol{r}\vec{<}\boldsymbol{r}_{i_o}$.' In the last two equations of (6) the tangential transversal fields (index t) are determined from their longitudinal counterparts (index x) by applying (4). The integral equations (6) consist of four continuity relations between $E_x(\boldsymbol{r})$ and $H_x(\boldsymbol{r})$ in four unknown functions $E_x(\boldsymbol{r}_j), H_x(\boldsymbol{r}_j), E_t(\boldsymbol{r}_j)$ and $H_t(\boldsymbol{r}_j)$. These unknowns are defined over the total boundary of all conductors $j, j = 1,\cdots,C$.

In the case of a perfect conductor we have that $E_x(\boldsymbol{r}_j) = E_t(\boldsymbol{r}_j) = 0$, or that only two unknown functions $H_x(\boldsymbol{r}_j)$ and $H_t(\boldsymbol{r}_j)$ do not vanish at the perfectly conducting boundaries. At these boundaries we can only impose two conditions: $E_x(\boldsymbol{r}\vec{>}\boldsymbol{r}_j) = E_t(\boldsymbol{r}\vec{>}\boldsymbol{r}_j) = 0$. This means that (6) reduces to a set of two equations with two unknown functions.

IV. Solution of the Integral Equation

A. Basis Functions and Test Functions

The integral equation (6) is solved with Galerkin's method. The basis and test functions in the moment method of Galerkin

are chosen in a natural way. We first concentrate on the basis functions. For H_x we use a piecewise linear representation and for H_t we use a piecewise constant representation. If we look at the first equation of (5) we see a term proportional to H_t and a term proportional to $\partial H_x/\partial t$. When H_x is piecewise linear, $\partial H_x/\partial t$ will be piecewise constant; so it would not make much sense to use a higher order representation for H_t. In the case of a perfect conductor H_t and H_x are equal to the surface currents on the conductor. In [5] the same choice of basis functions is used for the representation of the surface current. By analogy we use a piecewise linear representation for E_x and a piecewise constant representation for E_t.

As test functions in the method of Galerkin we use piecewise constant functions for E_x and H_x and piecewise linear functions for E_t and H_t. This choice of basis and test functions results in a very elegant and consistent development of the theory. We will come back to this point in the sequel.

The boundary of each conductor is divided into a number of segments with not necessary equal length. For the piecewise constant representation we use pulse functions $p(\tau)$ where τ is the arc length:

$$p(\tau) = \frac{1}{\delta} \qquad 0 \le \tau \le \delta. \tag{7}$$

Overlapping triangular functions $t(\tau)$ (see Fig. 4(a)) are used for the piecewise linear representation:

$$\begin{aligned} t(\tau) &= 1 + \frac{\tau}{\delta_1} \qquad -\delta_1 \le \tau \le 0 \\ &= 1 - \frac{\tau}{\delta_2} \qquad 0 \le \tau \le \delta_2 \end{aligned} \tag{8}$$

The total number of segments on all conductor boundaries is equal to N. $p_k(\tau)\tau \in [0, \delta_k]\,(k = 1, \cdots, N)$ denotes the kth pulse function and $t_k(\tau)\tau \in [-\delta_{1,k}, \delta_{2,k}]\,(k = 1, \cdots, N)$ denotes the kth triangular function.

The segment on a conductor corresponding to a specific basis function will be called excitation segment. A segment corresponding to a specific test function will be called observation segment. So each segment is sometimes seen as an excitation segment and sometimes as an observation segment depending on the context.

B. Discrete Eigenvalue Problem

If the total number of segments on all conductors is equal to N, our integral equation is discretised in a set of $4N$ homogeneous linear equations, each corresponding to a test function, with $4N$ unknown amplitudes of the basis functions shown in (9) at the bottom of the page. $E_{x,k}, H_{x,k}, E_{t,k}$ and $H_{t,k}\,(k = 1, \cdots, N)$ are the unknown amplitudes of the basis functions in the representation of E_x, H_x, E_t and H_t. $[XY]_{kl}\,(k, l = 1, \cdots, N;\ X, Y = E_x, H_x, E_t, H_t)$ is the X boundary condition tested at the kth observation segment and generated by the basis function of the field component Y at the lth excitation segment. So $[XY]_{kl}$ contains an integration over the lth excitation segment and over the kth observation segment. Comparison of (6) and (9) shows that $[XY]_{kl}$ is formed by the difference of an internal and external part and that this external part consists of an incoming and scattered contribution.

Each coefficient $[XY]_{kl}$ in (9) is a nonlinear function of the propagation constant β. (9) will only have nontrival solutions if the determinant of the system matrix vanishes. This determinant is a function of β and will become zero for some discrete values of β. These values correspond to the propagation constants of the eigenmodes and the corresponding solutions or eigenvectors of (9) are the eigenmode field components at the conductor boundaries.

C. The System Matrix

1. Space Domain: In this section we will give explicit expressions for the excitation and observation integration appearing in each coefficient of the system matrix. First the observation integration over the test function is examined followed by the excitation integration.

Each coefficient of type $[E_x Y]_{kl}$, with $Y = E_x, E_t, H_x$ or H_t, contains a test integration of E_x over the kth segment. This integration takes the form:

$$\int_0^{\delta_k} p_k(\nu)\, E_x(\boldsymbol{r}(\nu))\, d\nu \tag{10}$$

where $E_x(\boldsymbol{r})$ is the longitudinal electric field generated by the lth basis function of field component Y. $E_x(\boldsymbol{r})$ can be an

$$\begin{bmatrix} [E_xE_x]_{11} & \cdots & [E_xE_x]_{1N} & & [E_xH_t]_{11} & \cdots & [E_xH_t]_{1N} \\ \vdots & & \vdots & \cdots & \vdots & & \vdots \\ [E_xE_x]_{N1} & \cdots & [E_xE_x]_{NN} & & [E_xH_t]_{N1} & \cdots & [E_xH_t]_{NN} \\ [H_xE_x]_{11} & \cdots & [H_xE_x]_{1N} & & [H_xH_t]_{11} & \cdots & [H_xH_t]_{1N} \\ \vdots & & \vdots & \cdots & \vdots & & \vdots \\ [H_xE_x]_{N1} & \cdots & [H_xE_x]_{NN} & & [H_xH_t]_{N1} & \cdots & [H_xH_t]_{NN} \\ [E_tE_x]_{11} & \cdots & [E_tE_x]_{1N} & & [E_tH_t]_{11} & \cdots & [E_tH_t]_{1N} \\ \vdots & & \vdots & \cdots & \vdots & & \vdots \\ [E_tE_x]_{N1} & \cdots & [E_tE_x]_{NN} & & [E_tH_t]_{N1} & \cdots & [E_tH_t]_{NN} \\ [H_tE_x]_{11} & \cdots & [H_tE_x]_{1N} & & [H_tH_t]_{11} & \cdots & [H_tH_t]_{1N} \\ \vdots & & \vdots & \cdots & \vdots & & \vdots \\ [H_tE_x]_{N1} & \cdots & [H_tE_x]_{NN} & & [H_tH_t]_{N1} & \cdots & [H_tH_t]_{NN} \end{bmatrix} \begin{bmatrix} E_{x,1} \\ \vdots \\ E_{x,N} \\ H_{x,1} \\ \vdots \\ H_{x,N} \\ E_{t,1} \\ \vdots \\ E_{t,N} \\ H_{t,1} \\ \vdots \\ H_{t,N} \end{bmatrix} = \begin{bmatrix} 0 \\ \vdots \\ 0 \\ 0 \\ \vdots \\ 0 \\ 0 \\ \vdots \\ 0 \\ 0 \\ \vdots \\ 0 \end{bmatrix}. \tag{9}$$

incoming or scattered field. The expression for $[H_x Y]_{kl}$ is analogous to (10).

$[E_t Y]_{kl}$ on the other hand contains an integration of the form:

$$\int_{-\delta_{k,1}}^{\delta_{k,2}} t_k(\nu)\, E_t(\boldsymbol{r}(\nu))\, d\nu. \tag{11}$$

The transversal tangential field $E_t(\boldsymbol{r})$ has to be expressed in function of the basic field quantities using (4):

$$\int_{-\delta_{k,1}}^{\delta_{k,2}} t_k(\nu)\left[-\frac{j\beta}{\gamma^2}\frac{\partial E_x(\boldsymbol{r}(\nu))}{\partial t} + \frac{j\omega\mu}{\gamma^2}\frac{\partial H_x(\boldsymbol{r}(\nu))}{\partial n}\right] d\nu \tag{12}$$

$[H_t Y]_{kl}$ is again analogous to (12).

$[XE_x]_{kl}$, with $X = E_x, E_t, H_x$ or H_t, contains an integration over the lth basis function of the representation of E_x. The integrations associated with $[XE_x]_{kl}$ are

$$E_x^{\text{in}}(\boldsymbol{r}) = \int_{-\delta_{1,1}}^{\delta_{1,2}} t_1(\nu)\frac{\partial G(\boldsymbol{r}|\boldsymbol{r}'(\tau))}{\partial n'} d\tau \tag{13}$$

or:

$$H_x^{\text{in}}(\boldsymbol{r}) = -\frac{\beta}{\omega\mu}\int_{-\delta_{1,1}}^{\delta_{1,2}} \frac{dt_1(\tau)}{d\tau} G(\boldsymbol{r}|\boldsymbol{r}'(\tau))\, d\tau \tag{14}$$

as can be verified directly from (5). Analogous expressions hold for $[XH_x]_{kl}$. From (5) one sees that $[XE_t]_{kl}$ has only a magnetic contribution:

$$H_x^{\text{in}}(\boldsymbol{r}) = \frac{j\gamma^2}{\omega\mu}\int_0^{\delta_1} p_1(\tau)\, G(\boldsymbol{r}|\boldsymbol{r}'(\tau))\, d\tau \tag{15}$$

And finally $[XH_t]_{kl}$ is again analogous to (15).

2. *Spectral Domain:* The Hankel function in the Green's function $G(\boldsymbol{r}|\boldsymbol{r}') = j/4H_0^{(2)}(\gamma|\boldsymbol{r} - \boldsymbol{r}'|)$ and her derivatives appearing in (13)–(15) make the basis function integration difficult. This problem can be solved if we spatially Fourier transform the expressions (13)–(15) and calculate the spectral longitudinal incoming fields. Interchanging the Fourier transform with the excitation integration and possible normal derivatives (appearing in (13)) leads us to the Fourier transform of the Green's function. This Fourier transform is given by ([9] page 360):

$$\frac{1}{2\pi}\int_{-\infty}^{+\infty} G(\boldsymbol{r}|\boldsymbol{r}')e^{jk_y y}\, dy = -\frac{1}{4\pi}\frac{e^{jk_y y'}e^{-\Gamma|z-z'|}}{\Gamma} \qquad \Gamma = \sqrt{k_y^2 - \gamma^2}. \tag{16}$$

The y-direction is indicated on Fig. 1. This spectral Green's function allows us to perform the integration over the basis function analytically if the excitation segment is a straight line. The spectral incoming fields are also needed in the calculation of the scattered fields.

The space domain fields appearing in the test integrations (10) and (12) are found by inverse Fourier transforming the incoming or scattered spectral fields. We will however first bring the inverse Fourier transform outside the test function integration by interchanging both integrations. This makes it possible to perform also the test function integration analytically if the observation segment is a straight line and only the final inverse Fourier transform remains to be integrated numerically. Remark that we use this spectral technique even for internal regions with finite dimensions.

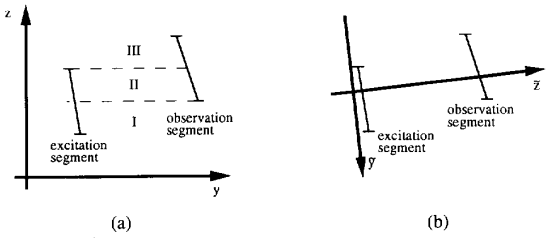

Fig. 3. Observation and excitation segment with overlapping z coordinates in the (y, z) coordinate system (Fig. 3(a)) and without overlapping $\tilde{z}$ coordinates in the new $(\tilde{y}, \tilde{z})$ coordinate system (Fig. 3(b)).

D. Incoming Coefficients

Even after applying the spectral domain technique the basis and test integrations can become pretty complicated. This is due to the absolute value of $|z - z'|$ appearing in the spectral Green's function (16). Consider a typical basis function integration over an excitation segment. If we need the spectral incoming fields at a z coordinate above or under the excitation segment there is no problem because $(z - z')$ has a fixed sign. However if we need the spectral incoming field at a z coordinate at the height of the excitation segment we have to divide the basis function integration in two parts: one with $|z - z'| = (z - z')$ and one with $|z - z'| = -(z - z')$. At the observation segment we integrate over z. This means that if the observation and excitation segment have overlapping z-coordinates, as shown in Fig. 3(a), we have to divide both integrations in several parts. In region I $(z - z')$ is positive, in region III $(z - z')$ is negative and in region II $(z - z')$ can have both signs and the basis and test integrations are coupled. However, this problem can be solved in an elegant way.

The incoming fields are fields generated in a homogeneous space of infinite extend, so there is no preferential spectral transformation direction imposed by the layered medium. If we use the new coordinate system $(\tilde{y}, \tilde{z})$ of Fig. 3(b) and if we Fourier transform along the new $\tilde{y}$ direction this partitioning in zones is no longer necessary because $(\tilde{z} - \tilde{z}')$ is always positive. A problem case occurs when the basis and test function coincide i.e. the so-called self-patch contribution. This problem can only be solved for polygonal waveguides in which case the $\tilde{y}$ axes is taken to be along the straight segment and $(\tilde{z} - \tilde{z}')$ is equal to zero. In the further calculation we will always use the standard (y, z) coordinate system, but for the incoming coefficients this system is assumed to be the $(\tilde{y}, \tilde{z})$ coordinate system.

E. Scattered Coefficients

As will be shown in the next section the spectral longitudinal incoming fields consist of terms of the following general form:

$$E_x^{\text{in}}(k_y, z) = e^{\pm}(k_y)e^{\pm\Gamma z}$$
$$H_x^{\text{in}}(k_y, z) = h^{\pm}(k_y)e^{\pm\Gamma z}. \tag{17}$$

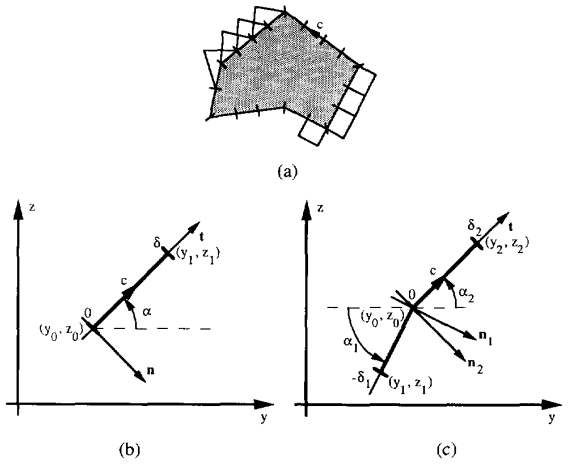

Fig. 4. Polygonal conductor (Fig. 4(a)) with its boundary divided in segments. Notations to handle pulse functions (Fig. 4(b)) and triangular functions (Fig. 4(c)).

In the spectral domain the layered medium can be seen as a TE and TM cascade of transmission lines. The incoming fields (17), after decomposition in TE and TM components, are represented as voltage and current sources in these cascades. Solution of the cascades with a matrix formalism described in [10] results in the TE and TM components of the scattered fields. After combination of both components, the spectral longitudinal scattered fields in each layer can be written in the following general form:

$$E_x^{sc}(k_y,z) = \tilde{e}^{+}(k_y)e^{\Gamma z} + \tilde{e}^{-}(k_y)e^{-\Gamma z}$$
$$H_x^{sc}(k_y,z) = \tilde{h}^{+}(k_y)e^{\Gamma z} + \tilde{h}^{-}(k_y)e^{-\Gamma z} \qquad (18)$$

The solution of the cascades, i.e. the relation between $\tilde{e}^{\pm}(k_y), \tilde{h}^{\pm}(k_y)$ and $e^{\pm}(k_y), h^{\pm}(k_y)$, has to be determined only once for each excitation-observation layer combination and not for each excition-observation segment combination. This means that the calculation time for scattered coefficients is only slightly higher than for incoming coefficients.

V. Basis and Test Function Integrations

In the further development of the theory it is necessary to assume conductors with polygonal cross-section. Fig. 4(a) represents a polygonal conductor with its boundary divided in segments. Corners of the boundary are always at the edges of segments. Fig. 4(b) shows the notations used to handle pulse basis and test functions. The triangular function case is shown in Fig. 4(c). Two angles α_1 and α_2 are introduced because a triangular segment can be across a corner of a conductor.

We start with the basis function integration, in other words we determine the spectral longitudinal incoming fields generated by each basis function. This means that the Fourier transforms in (13)–(15) are calculated. We will use the conditions $z > z'$ respectively $z < z'$, by this we mean that z must be taken above respectively under all the z' coordinates of the excitation segment.

We start with the contribution of a basis function for E_t to the longitudinal incoming magnetic field $H_x^{\text{in}}(k_y,z)$. This is the Fourier transform of (15). To simplify notations the subscript '1', referring to a specific basis function, is omitted. With the spectral Green's function (16) and the pulse function (7) one finds, when $z > z'$:

$$H_x^{\text{in}}(k_y,z) = -\frac{j\gamma^2 e^{-\Gamma z}}{4\pi\Gamma\mu\omega\delta}\int_0^{\delta} e^{ik_y y'}e^{\Gamma z'}\,d\tau \qquad (19)$$

with $y' = y_0 + \tau\cos\alpha$ and $z' = z_0 + \tau\sin\alpha$. Integrating (19) yields:

$$H_x^{\text{in}}(k_y,z) = -\frac{j\gamma^2 e^{-\Gamma z + m_0}(e^{\delta t}-1)}{4\pi\Gamma\mu\omega\delta t} \qquad (20)$$

with $m_0 = jk_y y_0 + \Gamma z_0$ and $t = jk_y\cos\alpha + \Gamma\sin\alpha$. The case when $z < z'$ is analogous and is left to the reader.

Now we concentrate on the E_x basis function contribution (13) to $E_x^{\text{in}}(k_y,z)$. In this case we need the normal derivative of the spectral Green's function. For this we use the following relations between the (t,n) and (y,z) derivatives:

$$\frac{\partial}{\partial n} = \sin\alpha\frac{\partial}{\partial y} - \cos\alpha\frac{\partial}{\partial z}$$
$$\frac{\partial}{\partial t} = \cos\alpha\frac{\partial}{\partial y} + \sin\alpha\frac{\partial}{\partial z}. \qquad (21)$$

For $z > z'$ the Fourier transform of the normal derivative of G is equal to

$$\frac{1}{2\pi}\int_{-\infty}^{+\infty}\frac{\partial G(\boldsymbol{r}|\boldsymbol{r}')}{\partial n'}e^{jk_y y}\,dy = -\frac{w}{4\pi}\frac{e^{jk_y y'}e^{-\Gamma(z-z')}}{\Gamma} \qquad (22)$$

where $w = jk_y\sin\alpha - \Gamma\cos\alpha$. $E_x^{\text{in}}(k_y,z)$ with (22) and (8) is given by

$$E_x^{\text{in}}(k_y,z) = -\frac{e^{-\Gamma z}}{4\pi\Gamma}\left[w_1\int_{-\delta_1}^{0}\left(1+\frac{\tau}{\delta_1}\right)e^{jk_y y'}e^{\Gamma z'}\,d\tau + w_2\int_0^{\delta_2}\left(1-\frac{\tau}{\delta_2}\right)e^{jk_y y'}e^{\Gamma z'}\,d\tau\right]. \qquad (23)$$

If we integrate by parts we finally find:

$$E_x^{\text{in}}(k_y,z) = -\frac{e^{-\Gamma z+m_0}}{4\pi\Gamma}\left[\frac{w_1(e^{-\delta_1 t_1}-1}{\delta_1 t_1^2} + \frac{w_2(e^{\delta_2 t_2}-1)}{\delta_2 t_2^2} + \frac{w_1}{t_1} - \frac{w_2}{t_2}\right], \qquad (24)$$

where t_1 and w_1 respectively t_2 and w_2 correspond to t and w with α replaced by α_1 respectively α_2. Note that for a straight excitation segment, without a corner at $\tau = 0, t_1$ and w_1 are respectively equal to t_2 and w_2. This means that in this case the last two terms in (24) cancel each other out. The $z < z'$ case is again left to the reader.

The calculation of the other contributions to $H_x^{\text{in}}(k_y,z)$ and $E_x^{\text{in}}(k_y,z)$ are analogous.

The test function integration is needed to apply Galerkin's procedure. The test integration is completely analogous to the procedure applied for the basis function integration after interchanging the test integration and the inverse Fourier transformation. For this reason we will not present an explicit calculation of this integration.

VI. Inverse Fourier Transformation

The spectral integration is performed in the classical way as described for example in [11]. For $k_y \in [-k_c, k_c]$ we use simple Gauss quadrature integration formulas along a suitable complex integration path. The asymptotic part of the integration, i.e. $k_y \in [k_c, +\infty[$ and $k_y \in]-\infty, -k_c]$, allows a special treatment. k_c is taken high enough to ensure that Γ can be approximated by $|k_y|$. We will concentrate on the positive part, $k_y \in [k_c, +\infty[$, of the asymptotic integration in which $\Gamma = k_y$.

From (20) and (24) it can be seen that the scattered longitudinal incoming fields contain only terms proportional to

$$\frac{e^{-ak_y}}{k_y^2} \quad \mathrm{Re}(a) \geq 0. \tag{25}$$

Note that the last two terms in (24) cancel out when we replace Γ by k_y. The common spectral asymptotic character (25) of all spectral longitudinal incoming fields is due to the special choice of the basis functions. Note that one factor $1/k_y$ is due to the spectral Green's function and one is due to the basis function integration. The integration over the test function will introduce an extra factor $1/k_y$. The fact that the test function integration always results in an extra factor $1/k_y$ is due to the special choice of the test functions.

First we concentrate on the asymptotic part of the incoming coefficients $[XY]_{kl}^{\mathrm{in},as}$ of the system matrix. From the above it is clear that these coefficients are the sum of terms of the following form:

$$[XY]_{kl}^{\mathrm{in},as} = C \int_{k_c}^{+\infty} \frac{e^{-ak_y}}{k_y^3} dk_y = \frac{C}{k_c^2} E_3(ak_c) \quad \mathrm{Re}(a) \geq 0. \tag{26}$$

With $E_3(x)$ the third order exponential integral ([9], p. 228).

The scattered coefficients $[XY]_{kl}^{sc,as}$ also contain the $1/k_y^3$ spectral character due to basis and test function integration. However due to the solution of the layered medium an extra function $f(k_y)$ is introduced which describes the propagation and reflection in the layers. So $[XY]_{kl}^{sc,as}$ can be written as a sum of terms of the following form:

$$[XY]_{kl}^{sc,as} = \int_{k_c}^{+\infty} f(k_y) \frac{e^{-ak_y}}{k_y^3} dk_y \quad \mathrm{Re}(a) \geq 0. \tag{27}$$

This integral can be evaluated with Gauss–Laguerre quadrature.

VII. Impedances

The complete circuit model requires the impedance matrix associated with the eigenmodi. In [12] this impedance matrix is calculated from the mode current in each conductor, the power propagated by each eigenmode and the cross powers between the eigenmodi.

It was not necessary to make any assumptions about the material parameters of the conductors for the calculation of the propagation constant. In order to give a meaningful interpretation to the total longitudinal current however, it is necessary to assume that the displacement current is negligible compared to the conduction current inside the conductors. The sufficiently high conductivity makes it also possible to restrict the power calculation to the layers and neglect the power propagated in the conductors.

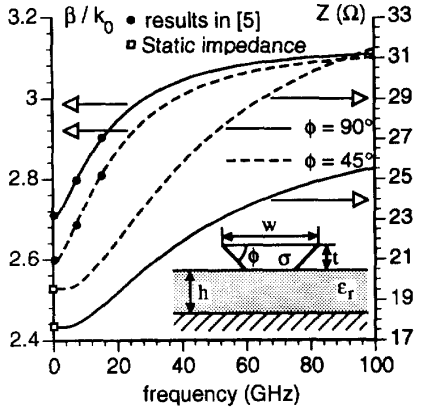

Fig. 5. Propagation constant and impedance as a function of frequency for a thick microstrip ($h = 0.635$ mm, and $w = 3.0$ mm, $t = 0.3$ mm, $\epsilon_r = 9.8, \sigma = \infty$).

The total longitudinal current I_j on conductor j ($j = 1, \cdots, C$) is calculated from the contour integral of the transversal tangential magnetic field H_t around the conductor surface because the displacement current in the conductor is neglected.

Suppose we want to calculate the cross-power P_{fg} propagated between mode f and mode g. This requires an integration of the x component of Poynting's vector over the cross-section of the waveguide. Using Parceval's theorem we can calculate P_{fg} in the spectral domain:

$$P_{fg} = \pi \int_{-\infty}^{+\infty} [E_{y,f}(k_y, z)\, H_{z,g}^*(k_y, z) - E_{z,f}(k_y, z)\, H_{y,g}^*(k_y, z)]\, dz\, dk_y. \tag{28}$$

For source-less layers, i.e., layers without conductors, the z-integration is calculated analytically.

In source layers things are more complicated. In principle it is possible to perform the z-integration, even in source layers, analytically. However this analytical integration results in very tedious expressions which would require enormous amounts of time to evaluate. Therefore we opted for a Gaussian quadrature numerical integration to perform the z- integration.

VIII. Numerical Examples

A. Microstrip Configuration

As first example we consider a thick microstrip (see inset of Fig. 5) with rectangular or trapezoidal cross-section on a substrate with thickness $h = 0.635$ mm and relative dielectric constant $\epsilon_r = 9.8$. The thickness t is one tenth of the top width $w = 3.0$ mm of the strip.

Fig. 5 presents the propagation characteristics of a perfectly conducting strip with rectangular ($\phi = 90°$) and trapezoidal ($\phi = 45°$) cross-section. The normalized propagation

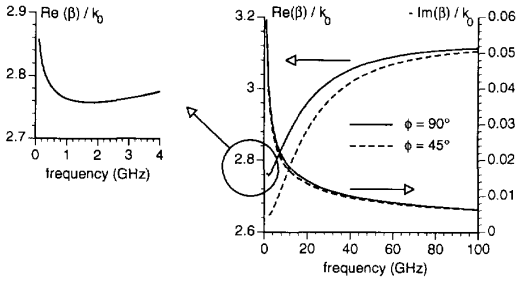

Fig. 6. Real and imaginary part of the propagation constant as a function of frequency for the strip of Fig. 5 with $\sigma = 100$ kS/m.

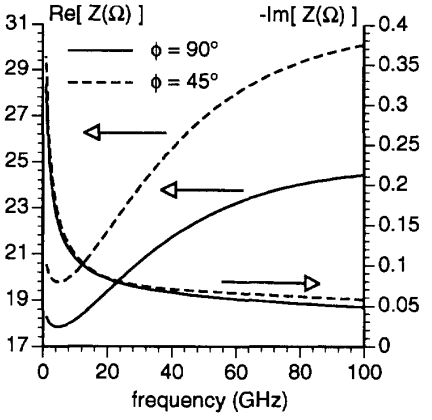

Fig. 7. Real and imaginary part of the impedance as a function of frequency of the strip of Fig. 5 with $\sigma = 100$ kS/m.

constants are found to be in excellent agreement with the results of Michalski and Zheng in [5]. We verified the low-frequency limits of the impedances with results obtained by our capacitance program described in [3].

In Figs. 6 and 7 the complex propagation constants' respective complex impedances are shown when the strip has a conductivity $\sigma = 100$ kS/m. This corresponds to a bad conductor worser than iron. As expected the attenuation constant $(= -\mathrm{Im}(\beta))$ decreases with increasing frequency as a result of the skin effect. At low frequencies the real part of the propagation constant shows a small dip (see enlargement on Fig. 6). This increase of $\mathrm{Re}(\beta)$ with decreasing frequency is a result of the fact that the fields start to penetrate deep inside the strip with high complex permittivity $\epsilon_r = \sigma/j\omega\epsilon_0$. Indeed, at 1 GHz the skin depth is 50.3 μm and at 100 MHz it has already increased to 159 μm which corresponds to half the strip thickness. In this frequency range perturbation techniques based on the skin effect are not applicable for this example. Remark also that $\mathrm{Re}(\beta)$ becomes almost equal to the propagation constant in the lossless case (Fig. 5) for frequencies above 8 GHz. The unbound character of $\mathrm{Im}(\beta)/k_0$ at $f = 0$ finds its origin in the factor f from $k_0 = 2\pi f\sqrt{\epsilon_0\mu_0}$. The dispersion curves (Fig. 7) for the impedance show the same properties as Fig. 6.

We have divided the strip of Fig. 5 in two smaller perfectly conducting strips (see inset of Fig. 8) with $w = 1$ mm

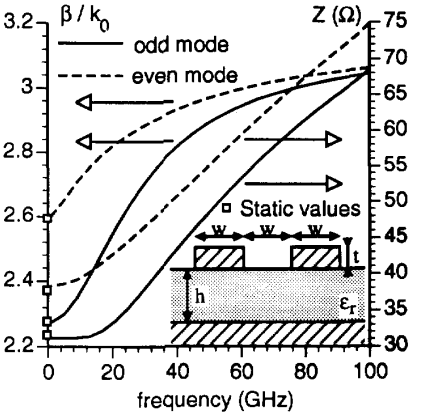

Fig. 8. Propagation constant and impedance as a function of frequency for the even and odd mode of two coupled microstrips ($h = 0.635$ mm, $w = 1.0$ mm, $t = 0.3$ mm, $\epsilon_r = 9.8$).

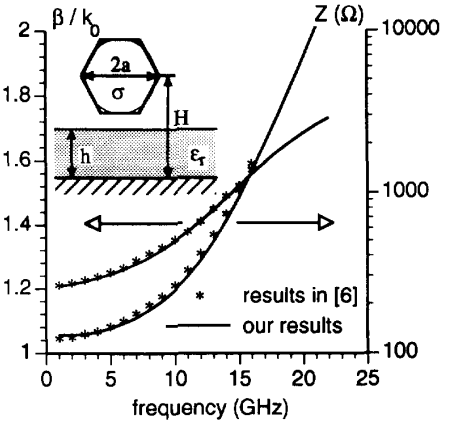

Fig. 9. Propagation constant and impedance as a function of frequency for a wire ($h = 3$ mm, $a = 0.75$ mm, $\epsilon_r = 4, \sigma = \infty, H = 4.5$ mm).

and $t = 0.3$ mm. Fig. 8 presents the dispersion curves for the propagation constants and impedances of the even and odd mode. The statical values obtained with our capacitance program are also indicated.

B. Wire Transmission Lines

The inset of Fig. 9 represents a wire with radius $a = 0.75$ mm approximated by an hexagon with the same area. The substrate has a thickness $h = 3$ mm and a relative dielectric constant $\epsilon_r = 4$. H is the distance between the center of the wire and the ground plane. In the simulations we used only two divisions on each side of the hexagon.

First we consider a perfectly conducting wire above the substrate with $H = 4.5$ mm. Fig. 9 shows the propagation constant and impedance dispersion curves compared with results obtained in [6] for round wires. Remark that the sudden increase of the impedance found in [6] is confirmed here. Slight differences in both impedance curves are probably due to fact that in [6] the power propagated in the source layer is determined in the space domain with a crude integration

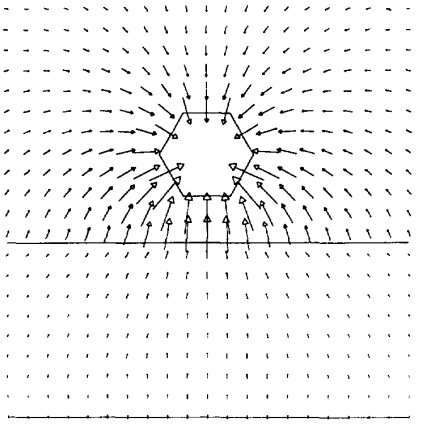

Fig. 10. Transversal electric field distribution around the wire of Fig. 9 with $\sigma = \infty$ and $H = 4.5$ mm at a frequency of 2 GHz.

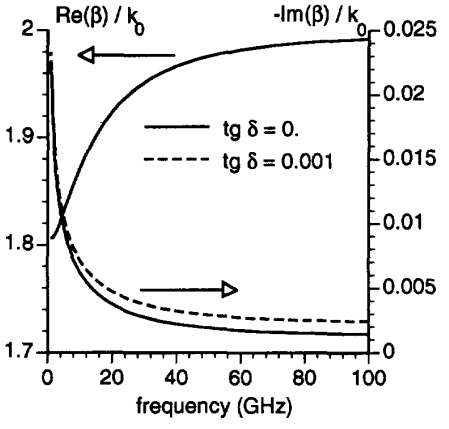

Fig. 11. Real and imaginary part of the propagation constant as a function of frequency for the wire of Fig. 9 with $\sigma = 100$ kS/m and $H = 3$ mm for two different values of the loss tangent of the substrate.

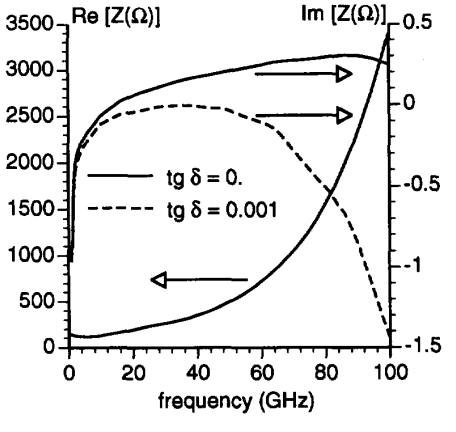

Fig. 12. Real and imaginary part of the impedance as a function of frequency for the wire of Fig. 9 with $\sigma = 100$ kS/m and $H = 3$ mm for two different values of the loss tangent of the substrate.

scheme. Fig. 10 shows an arrowplot of the transversal electric field components at a frequency of 2 GHz.

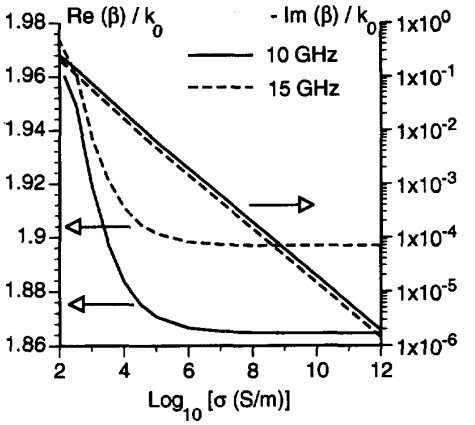

Fig. 13. Real and imaginary part of the propagation constant as a function of the conductivity σ for the wire of Fig. 9 with $H = 3$ mm.

Now we take $H = 3$ mm such that the wire is semi burried in the substrate. Figs. 11 and 12 show the complex propagation constants and impedances as a function of frequency when the wire has a conductivity $\sigma = 100$ kS/m for two different values of the loss tangent of the substrate ($tg\,\delta = 0.$ and $tg\,\delta = 0.001$). Note that the curves for the real part of both β and Z practically coincide for the two values of $tg\,\delta$. The imaginary part of Z shows the effect of losses in the conductor at low frequencies and the effect of losses in the substrate at high frequencies. Fig. 13 shows the propagation constant as a function of the conductivity σ of the wire for a frequency $f = 10$ GHz and $f = 15$ GHz and a lossless substrate.

REFERENCES

[1] C. Wei, R. F. Harrington, J. R. Mautz, and T. K. Sarkar, "Multiconductor transmission lines in multilayered dielectric media," *IEEE Trans. Microwave Theory Tech.*, vol. MTT-32, pp. 439–450, Apr. 1984.

[2] R. F. Harrington and C. Wei, "Losses on multiconductor transmission lines in multilayered dielectric media," *IEEE Trans. Microwave Theory Tech.*, vol. MTT-32, pp. 705–710, July 1984.

[3] F. Olyslager, N. Faché, and D. De Zutter, "New fast and accurate line parameter calculation of general multiconductor transmission lines in multilayered media," *IEEE Trans. Microwave Theory Tech.*, vol. 39, pp. 901–909, June 1991.

[4] J. J. Yang, G. E. Howard, and Y. L. Chow, "Complex image method for analyzing multiconductor transmission lines in multilayered dielectric media," in *1991 Int. Symp. IEEE Antennas and Propagation Symp. Dig.*, London, ON, Canada, vol. II, June 1991, pp. 862–865.

[5] K. A. Michalski and D. Zheng, "Rigorous analysis of open microstrip lines of arbitrary cross-section in bound and leaky regimes," *IEEE Trans. Microwave Theory Tech.*, vol. 37, pp. 2005–2010, Dec. 1989.

[6] N. Faché, F. Olyslager, and D. De Zutter, "Full-wave analysis of coupled perfectly conducting wires in a multilayered medium," *IEEE Trans. Microwave Theory Tech.*, vol. 39, pp. 673–681, Apr. 1991.

[7] S. Tedjini, N. Daoud, D. Rauly, and E. Pic, "Analysis of MMICs with finite strip thickness and conductivity," *Electron. Lett.*, vol. 24, pp. 965–966, July 1988.

[8] D. Nghiem, J. T. Williams, and D. R. Jackson, "A general analysis of propagation along multiple-layer superconducting stripline and microstrip transmission lines," *IEEE Trans. Microwave Theory Tech.*, vol. 39, pp. 1553–1565, Sept. 1991.

[9] M. Abramowitz and I. A. Stegun, *Handbook of Mathematical Functions with Formulas, Graphs and Mathematical Tables*. New York: Dover, 1970.

[10] N. Faché, J. Van Hese, and D. De Zutter, "Generalised space domain Green's dyadic for multilayered media with special application to microwave interconnections," *J. Electromagn. Waves Appl.*, vol. 3, no. 7, pp. 651–669, 1989.

[11] N. Faché and D. De Zutter, "Rigorous full-wave space domain solution for dispersive microstrip lines," *IEEE Trans. Microwave Theory Tech.*, vol. 36, pp. 731–737, Apr. 1988.
[12] N. Faché and D. De Zutter, "New high-frequency circuit model for coupled lossless and lossy waveguide structures," *IEEE Trans. Microwave Theory Tech.*, vol. 38, pp. 252–259, Mar. 1990.

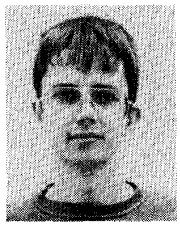

Frank Olyslager was born in Wilrijk, Belgium, on November 24, 1966. He received the degree in electrical engineering from the University of Ghent in July 1991. At present he is working toward the Ph.D. degree in electrical engineering at the University of Ghent as a Research Assistant of the National Fund for Scientific Research of Belgium. His research concerns the electromagnetic modeling of high-frequency electrical and optical interconnections.

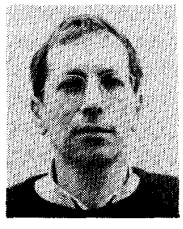

Daniël De Zutter was born in Eeklo, Belgium on November 8, 1953. He received the degree in electrical engineering from the University of Ghent in July 1976. From September 1976 to September 1984 he was a research and teaching assistant in the Laboratory of Electromagnetism and Acoustics (LEA) at the same university. In October 1981 he obtained a Ph.D degree there and in the spring of 1984 he completed a thesis leading to a degree equivalent to the French Aggrégation or the German Habilitation.

He is now a professor at Ghent University and Research Director at the National Science Foundation of Belgium. Most of his earlier scientific work dealt with the electrodynamics of moving media, with emphasis on the Doppler effect and Lorentz forces. His research now focuses on all aspects of circuit and electromagnetic modelling of high-speed and high-frequency interconnections.

In 1990 Dr. De Zutter was elected as a member of the Electromagnetics Society.

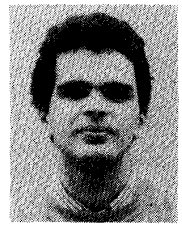

Krist Blomme was born in Eeklo, Belgium, on October 17, 1968. He received the degree in electrical engineering from the University of Ghent in July 1991. At present he is working toward the Ph.D. degree in electrical engineering at the University of Ghent as a Research Assistant of the National Fund for Scientific Research of Belgium. His research concerns electromagnetic modeling of high-frequency interconnection patterns with special attention to via holes.